CORROSION BEHAVIOR OF Fe-Al LAYERS IN SEAWATER CHARACTERIZED WITH ELECTROCHEMICAL IMPEDANCE SPECTROSCOPY

KARAKTERIZACIJA KOROZIJSKEGA OBNAŠANJA Fe-Al PLASTI V MORSKI VODI Z ELEKTROKEMIČNO IMPEDANČNO SPEKTROSKOPIJO

Ningning Li[1,2], Guang Chen[2]*, Xi Chen[1], Jiajia Yang[1], Liang Huang[1]

[1]School of Materials Science and Engineering, North China University of Water Resources and Electric Power, Zhengzhou 450045, P. R. China
[2]MIIT Key Laboratory of Advanced Metallic and Intermetallic Materials Technology, Engineering Research Center of Materials Behavior and Design, Ministry of Education, Nanjing University of Science and Technology, Nanjing 210094, P. R. China

The corrosion behavior of Fe-Al layers in artificial seawater was studied using electrochemical impedance spectroscopy (EIS). The layers were previously prepared on a Q235 low-carbon steel surface. Results show that there are two capacitive arcs during the whole immersion of the Fe-Al layers, fabricated at 650 °C and 750 °C. The two capacitive arcs represent two chemical reactions. The Fe-Al layer was the sacrificial anode, used for the cathodic protection. The results illustrate that the Fe-Al layer fabricated at 750 °C exhibited a better corrosion performance as it was protected by the passive film during the long immersion.

Keywords: Fe-Al layer, electrochemical impedance spectroscopy, corrosion behavior, sacrificial anode

Avtorji v članku opisujejo študijo korozijskega obnašanja Fe-Al plasti v umetni morski vodi. Teste so izvajali z elektrokemično impedančno spektroskopijo (EIS). Plasti so predhodno nanesli na površino malo-ogljičnega jekla Q235. Rezultati študije so pokazali, da sta nastala dva kapacitivna obloka pri popolni potopitvi Fe-Al plasti, ki sta bili izdelani pri 650 °C in 750 °C. Ta dva kapacitivna obloka so pripisali dvema kemičnima reakcijama in Fe-Al plast je igrala vlogo žrtvovane anode, kar vodi do katodne zaščite. Rezultati študije so pokazali, da ima Fe-Al plast, izdelana pri 750 °C boljše protikorozijske lastnosti, ker na njej nastaja trajnejši zaščitni (pasivni) film pri daljšem času potapljanja plasti v umetno morsko vodo.

Ključne besede: Fe-Al plast, elektrokemična impedančna spektroskopija, korozijsko obnašanje, žrtvovana anoda

1 INTRODUCTION

Fe–Al intermetallic compounds are often used as the traditional engineering materials due to their low density, high-temperature strength, outstanding oxidation and corrosion resistance.[1–3] In recent years, many studies have been carried out, leading to a lot of progress in the applications of Fe-Al as a protective surface layer, prepared with various methods. For instance, M. Emami et al.[1] researched an aluminized layer fabricated by hot-dip aluminizing, with the phases including Fe_2Al_5 and $FeAl_3$. Some other scholars have also made a comprehensive research into plasma aluminizing, slurry aluminizing and mechanical alloying.[2–6] Moreover, pack aluminizing is a commonly used method for obtaining an Fe-Al layer[7,8] as an in-situ chemical vapor deposition (CVD) process, which has the advantages of a simple operation, stable process and good quality. Z. L. Zhan et al.[7] discussed the microstructure and high-temperature oxidation of an aluminide coating, produced on carbon steel with a combination of surface refinement and pack aluminizing.

Just like all the methods mentioned above, individual properties of an Fe-Al layer were also researched, specifically the high-temperature oxidation and sulfidation corrosion[9–11] in addition to wear.[12] The aqueous corrosion behavior at room temperature of Fe-Al layers made with methods other than pack aluminizing, was also studied. Typically, X. L. Zhu et al.[13] discussed the corrosion properties of Fe-Al layers in the Na_2S and Na_2SO_4 + NaCl solutions, fabricated with double-glow plasma surface alloying. An Fe-Al layer has a potential application in the marine environment and electrochemical measurement, particularly with electrochemical impedance spectroscopy (EIS), which is commonly used to characterize the corrosion behavior in artificial seawater.[14,15]

In the initial research, the potentiodynamic polarization curves and weight-loss method were used to characterize the corrosion behavior of an Fe-Al layer in artificial seawater, as described in reference.[16] The aim of this work is to investigate the corrosion behavior of Fe-Al layers with the EIS method to verify the previous conclusions.

---
*Corresponding author's e-mail:
gchen@njust.edu.cn (Guang Chen)

2 EXPERIMENTAL PART

2.1 Materials preparation

The substrates were low-carbon steels (Q235) with the nominal chemical composition shown in **Table 1**. The substrates were aluminized at 650 °C or 750 °C for 20 h after the pretreatment, with the pack-powder mixture of 8Al-87Al$_2$O$_3$-5AlCl$_3$ (w/%). Detailed experimental procedures and results had been described elsewhere.[16] The preliminary main outcomes were summarized as follows: the content of Al in the Fe-Al layer fabricated at 650 °C (73.02 a/%) is slightly higher than that at 750 °C (72.49 a/%) and both layers include the Fe$_2$Al$_5$ and FeAl$_3$ phases. It means that the Fe-Al layer formed at 750 °C contained more Fe$_2$Al$_5$ phase than that formed at 650 °C. Specifically, the experiment included phase testing, cross-sectional morphology and element-content distribution, while further details can be found in reference.[16]

Table 1: Nominal chemical composition of the Q235 low-carbon steel (w/%)

Composition	Content
C	0.140–0.220
Mn	0.300–0.650
Si	0.300
S	≤0.050
P	0.045
Fe	Bal

2.2 Electrochemical measurements

The electrochemical measurements were performed with a conventional three-electrode system, using a CHI604D-type (Chenhua, Shanghai, China) electrochemical workstation at room temperature. The samples were embedded in epoxy resin with an exposed area of 1 cm^2 ($L \times W$), used as the working electrode. A saturated calomel electrode (SCE) served as the reference electrode, while the Pt electrode was the counter electrode. The solution for the electrochemical corrosion tests was artificial seawater, whose composition is shown in **Table 2** according to GB/T 17848-1999 (China).[17]

**Table 2:** Chemical composition of artificial seawater (g/L)

Composition	Content (g/L)
NaCl	24.530
MgCl$_2$·6H$_2$O	11.110
Na$_2$SO$_4$	4.090
CaCl$_2$	1.160
KCl	0.700
NaHCO$_3$	0.200
KBr	0.100
SrCl$_2$·6H$_2$O	0.042
NaF	0.003
H$_3$BO$_3$	0.027

Before the electrochemical tests, all the samples were immersed in the electrolyte solution for 30 min. The EIS was carried out at a frequency range of 0.1–100000 Hz and the amplitude was 5 mV. During all the experiments, the samples were immersed in artificial seawater at room temperature for a total of 30 days. After (2, 12, 24, 72, 120, 240, 480 and 720) h, the samples were tested with the EIS method. The solution was refreshed every seven days during the soaking period. After that, equivalent circuit models were adapted to acquire more information, which was analyzed with the ZSimpWin software, in order to further discuss the corrosion resistance of the aluminized layer.

3 RESULTS AND DISCUSSION

3.1 EIS results

Figures 1 and **2** show typical Nyquist and Bode plots, obtained after the EIS test of the Fe-Al layer fabricated at 650 °C. There are a big capacitive arc in the initial 2 h (**Figure 1a**) and arcs for 12 h and 24 h (the large image in **Figure 1b**). The capacitive-arc radius gradually decreases until the 720th h. Thus, it can be inferred that the capacitive arc for the early 2 h should be the superposition of the other two capacitive arcs, which is also illustrated by the two peaks on the Bode plots (**Figure 2b**). Two capacitive arcs represent two time constants, which further illustrate two interfaces. To be more specific, one refers to the passive film and electrolyte solution, the other refers to the passive film and aluminized layer surface. A. Ashrafi et al.[18] studied the passive-film
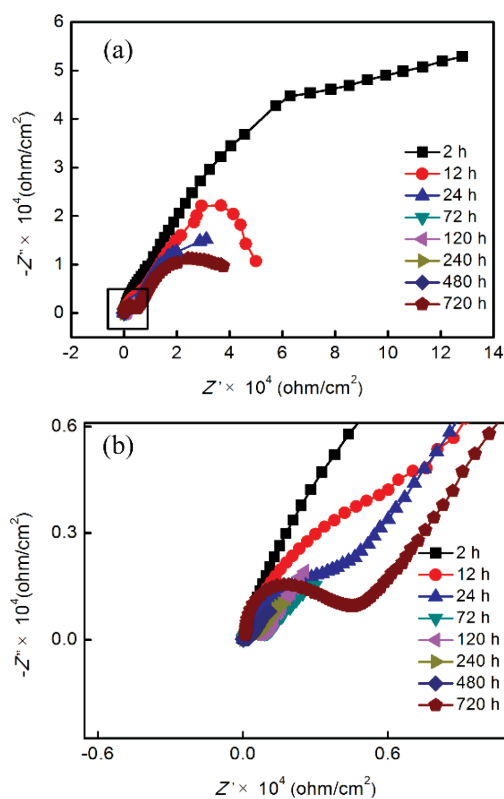
Figure 1: Nyquist plots of the Fe-Al layer fabricated at 650 °C: a) original image, b) larger image
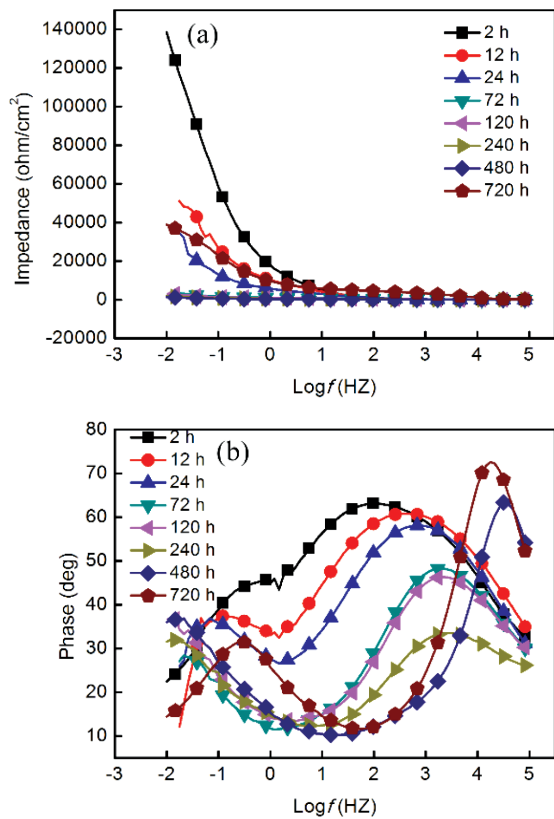
Figure 2: Bode plots of the Fe-Al layer fabricated at 650 °C: a) impedance, b) phase

Figure 3: Nyquist plots of the Fe-Al layer fabricated at 750 °C: a) original image, b) larger image

formation on mild steel in an oxalic acid solution tested with EIS, and also described the meaning of the two time constants, one being the metal/oxide interface and the other being the oxide/solution interface.

It can also be concluded that the passive-film formation is indicated by the high-frequency region in the Bode plots. A high-frequency region represents a chemical reaction between the original aluminized layer surface and solution. On the contrary, a damage process is related to a low-frequency zone. The impedance values are decreased at first and then increased as shown in **Figure 2a**. The phase angle is shown in **Figure 2b**. As a general rule, the larger the phase angle, the more complete is the passive film. On the contrary, the smaller the phase angle, the more broken is the passive film. Generally speaking, the Fe-Al layer surface is unstable during the immersion due to the trend change in the impedance and phase angle.

As shown in **Figures 3** and **4**, the same method was applied to the Fe-Al layer fabricated at 750 °C. The most obvious difference is in the Nyquist plots, which have two arcs during and after the 12th h, as shown in **Figure 3a**. In addition, the left high-frequency capacitive-arc radiuses are gradually reduced, as shown in **Figure 3b**, which is caused by the destroyed passive film. The right low-frequency capacitive arc is not obvious after 2 h because the initial corrosion behavior has not yet fully developed. Later, the low-frequency capacitive arc emerges
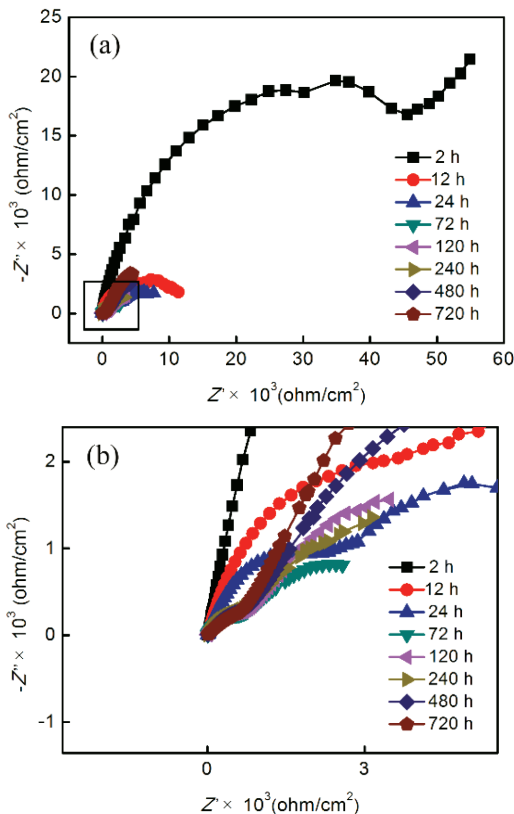

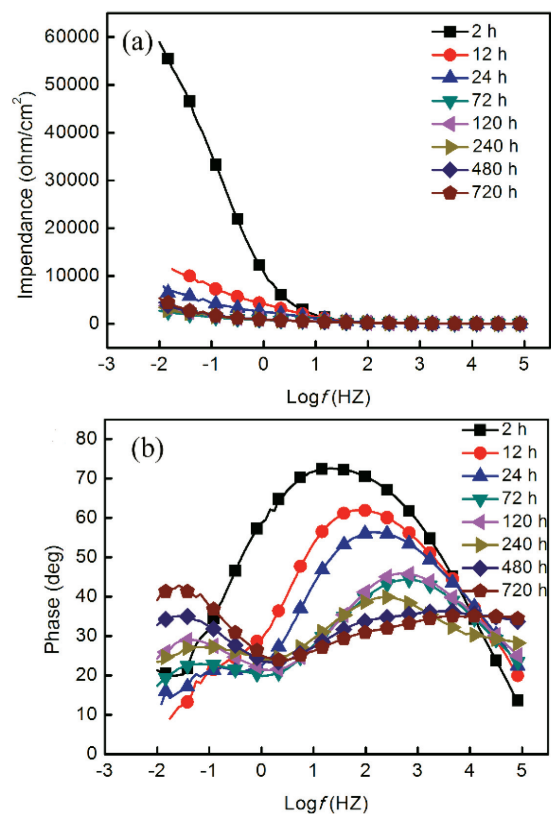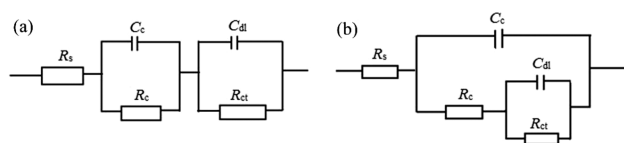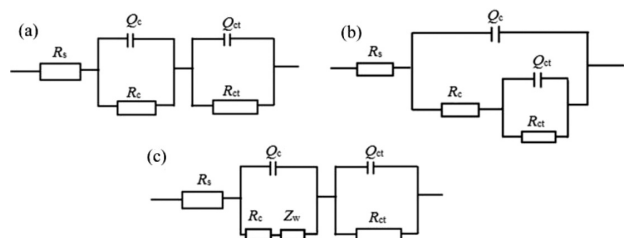**Figure 4:** Bode plots of the Fe-Al layer fabricated at 750 °C: a) impedance, b) phase

Figure 5: Common equivalent circuit models of two time constants: a) $R(CR)(CR)$, b) $R(C(R(CR)))$

Figure 6: Equivalent-circuit models of the Fe-Al layer fabricated at 650 °C for different immersion times

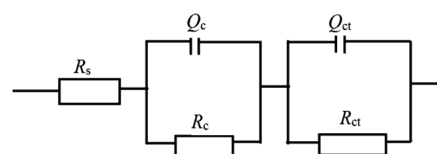Figure 7: Equivalent-circuit models of the Fe-Al layer fabricated at 750 °C

gradually. At the same time, the two capacitive arcs correspond to the two time constants, two interfaces and two essential chemical reactions.

The impedance values of the Bode plots first decrease and then remain stable in **Figure 4a**. On the other hand, the phase-angle values at a high frequency gradually descend with the prolonged reaction time in **Figure 4b**. However, the phase angle at a low frequency is not clear at the beginning, but develops after 12 h. The two peaks still correspond to the two time constants. The reason for the corrosion behavior will be discussed later.

3.2 Equivalent circuits

As it is known to all, the EIS results can be simulated with various equivalent circuits and the ones most frequently used are shown in **Figure 5**, corresponding to the two time constants. As shown in **Figure 5a**, this model is applied to the electrolyte-solution uniform seeping into the aluminized layer. However, the model from **Figure 5b** is suitable for the electrolyte solution seeping into the interface of the passive film and aluminized layer. The charging and discharging of the Fe-Al layer, except for the corroded passive-film, are not affected by the mass-transfer process.

As a matter of fact, the diffusion effect often exists, so the equivalent-circuit models need to be modified,

most clearly replacing C with the constant phase-angle element (CPE) that is Q. The adjusted models are shown in **Figures 6** and **7**. The component symbols represent the following: R_s is the solution resistance, Q_c is the capacitance of the original Fe-Al layer surface, including the passive film and later the corrosion products. R_c is the resistance of the passive film or corrosion products on the Fe-Al layer surface. Q_{ct} is the new electric double-layer capacitor, contacting the corrosive medium through pores. R_{ct} is the charge-transfer resistance at the surface and electrolyte interface. Y_0 ($\Omega \cdot cm^{-2} \cdot s^n$) and n ($0 \leq n \leq 1$) are the two parameters that characterize Q_{ct} and Q_c. Y_0 represents the base admittance of CPE, while n is the exponent, which can be used as the gauge of surface heterogeneity.[19] When more corrosion products are formed on the surface, they result in the approximate wireless length of the diffusion path and then the usual Warburg impedance appears. Z_w is the resistance symbol.

The $R(QR)(QR)$ model is suitable for etching after 2 h and 720 h, the $R(Q(R(QR)))$ model is suitable for the period of 12–72 h, while the $R(Q(RW)(QR))$ model is suitable for the period of 120–480 h, as shown in **Figures 6a** to **6c**. In the first two hours, the seawater is infiltrated uniformly. In the period of 12–72 h, the electrolyte solution is in contact with the interface between the passive film and aluminized layer; after the passive film is destroyed, corrosion products appear. The iron and aluminum products affect the corrosion process. Therefore, corrosion is caused by the corrosion-product accumulation, controlled by charge transfer and diffusion between 120 h and 480 h. However, diffusion is still the main controlling factor. It is clear that the corrosion behavior of the Fe-Al layer fabricated at 650 °C is controlled by the charge transfer and diffusion. This is also confirmed with the R_{ct} values from **Table 3**. That is to say, the corrosion first increased and then decreased, but increased again. At the same time, the effect of corrosion products

Table 3: EIS parameters of the aluminized layer fabricated at 650 °C and immersed in seawater for different times

Time (h)	R_s	Q_c		R_c	Z_w	Q_{ct}		R_{ct}
	$\Omega \cdot cm^{-2}$	Y_0 ($\Omega \cdot cm^{-2} \cdot s^n$)	n	$\Omega \cdot cm^{-2}$		Y_0 ($\Omega \cdot cm^{-2} \cdot s^n$)	n	$\Omega \cdot cm^{-2}$
2	12.450	1.925×10^{-5}	0.6497	1.803×10^5	–	1.050×10^{-5}	0.9335	3.649×10^3
12	10.510	9.999×10^{-6}	0.6992	1.162×10^4	–	4.444×10^{-5}	0.7714	5.330×10^4
24	13.000	1.088×10^{-5}	0.6916	4.854×10^3	–	1.041×10^{-4}	0.6358	5.346×10^4
72	12.020	1.878×10^{-5}	0.6481	8.554×10^2	–	1.407×10^{-3}	0.4859	1.785×10^4
120	9.285	7.793×10^{-6}	0.8759	1.888×10^2	1.479×10^{-3}	8.350×10^{-5}	0.5265	5.629×10^2
240	7.542	4.685×10^{-4}	0.3479	4.159×10^2	1.844×10^{-3}	2.273×10^{-5}	0.7390	1.509×10^2
480	4.360	6.363×10^{-5}	0.6343	1.486×10^2	3.356×10^{-3}	2.463×10^{-7}	0.9210	82.49
720	64.770	3.337×10^{-8}	0.9356	3.790×10^3	–	4.905×10^{-5}	0.5259	5.4070×10^4

Table 4: EIS parameters of the aluminized layer fabricated at 750 °C and immersed in seawater for different times

Time (h)	R_s	Q_c			R_c	Q_{ct}		R_{ct}
	Ω cm^{-2}	$Y_0(\Omega$ cm$^{-2}\cdot$s$^n)$	n		Ω cm^{-2}	$Y_0(\Omega$ cm$^{-2}\cdot$s$^n)$	n	Ω cm^{-2}
2	6.889	1.070×10^{-4}	0.6631		6.2530×10^4	2.181×10^{-5}	0.8819	2.8440×10^4
12	6.435	2.620×10^{-5}	0.8868		2.213×10^3	1.342×10^{-4}	0.5842	1.0800×10^4
24	5.861	3.386×10^{-5}	0.7938		1.585×10^3	3.167×10^{-4}	0.5051	8.551×10^3
72	6.684	1.212×10^{-4}	0.5680		7.165×10^2	1.317×10^{-3}	0.5976	3.149×10^3
120	5.358	8.557×10^{-4}	0.4188		3.1540×10^4	6.909×10^{-5}	0.6848	4.457×10^2
240	3.528	7.251×10^{-4}	0.3662		1.7410×10^4	9.628×10^{-5}	0.7698	2.264×10^2
480	2.828	1.179×10^{-3}	0.6845		8.833×10^3	2.220×10^{-4}	0.4411	1.089×10^3
720	1.211	2.547×10^{-4}	0.4157		9.496×10^2	1.022×10^{-3}	0.6946	1.4600×10^4

on the corrosion property is illustrated with the Warburg impedance Z_w.

The updated equivalent-circuit model of the Fe-Al layer fabricated at 750 °C is shown in **Figure 7**. The symbols of the components were described above. The $R(QR)(QR)$ model also indicates that the seawater infiltrated uniformly. According to the fitting results, the Warburg impedance is not observed, so the corrosion products had no influence on the corrosion, and the whole immersion was controlled by the charge transfer. The fitted data is shown in **Table 4**. It is different from the data obtained earlier. The value of R_{ct} reflects the corrosion resistance. That is, the larger the R_{ct}, the better is the corrosion resistance.
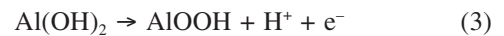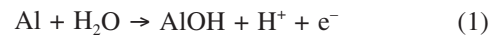
3.3 Corrosion mechanism

As stated in reference,[16] pitting corrosion is found with two methods. One is creating a polarization curve, the other is determining the weight loss. However, the effect of the corrosion products on the erosion process is not described. Based on the EIS results, the corrosion mechanism can be obtained as shown in **Figure 8**.
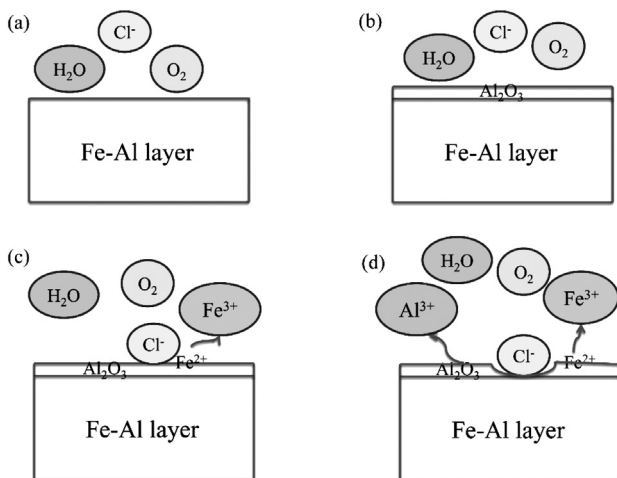
It is generally known that aluminum exhibits a strong corrosion activity. When Al contacts the oxygen atoms in water, the alumina passive film immediately becomes oxidized (**Figures 8a** and **8b**). In seawater, chloride ion, that is, Cl$^-$ is the most corrosive. However, the passive film is destroyed when it meets Cl$^-$. Meanwhile, the iron atoms go through a similar process, maintaining the charge stable (**Figure 8c**). Finally, pitting arises (**Figure 8d**). In this way, the aluminized layer can be used as the sacrificial anode, providing for the cathodic protection of low-carbon steel. The main chemical reactions for the passive film are as follows:

$$Al + H_2O \rightarrow AlOH + H^+ + e^- \qquad (1)$$

$$AlOH + H_2O \rightarrow Al(OH)_2 + H^+ + e^- \qquad (2)$$

$$Al(OH)_2 \rightarrow AlOOH + H^+ + e^- \qquad (3)$$

When the Cl$^-$ ions begin to surround and dissolve metal ions, the typical reactions are as follows:

$$AlOH + Cl^- \rightarrow AlOHCl + e^- \qquad (4)$$

$$AlOHCl + Cl^- \rightarrow AlOHCl_2 + e^- \qquad (5)$$

As described above, after the 120-h immersion, the aluminized layer fabricated at 650 °C is influenced by the corrosion products, as illustrated with the Warburg impedance Z_w. The self-sealing effect caused by the corrosion products leads to an increased resistance. Within this process, there is a synergistic effect of the passive film and corrosion products on the aluminized-layer surface. The total erosion is affected by the charge transfer and diffusion. However, the products have no obvious effect on the corrosion resistance of the layer fabricated at 750 °C and the whole erosion is protected by the passive film. In addition, the charge transfer is the dominating process.

From the above data, it can be seen that the Fe-Al layer can improve the corrosion resistance of a steel substrate. The layer prepared at 750 °C exhibits a better performance, which is consistent with the results acquired from other references.[16] This may be due to its strong ability to form a passive film, namely alumina.

Figure 8: Schematic diagram of the corrosion mechanism of the Fe-Al layer in seawater: a) Fe-Al layer in touch with seawater, b) Al$_2$O$_3$ passive film formed, c) chlorine ion reacting with the passive film and the iron ions produced, d) etching pits emerged

4 CONCLUSIONS

(1) There are two capacitive arcs obtained with the Nyquist and Bode plots of the two Fe-Al layers, representing two reactions; one is the formation of a passive film, the other is the destruction of the passive film.

(2) The layer fabricated at 750 °C exhibits a better corrosion resistance. This is due to the alumina passive film functioning as the sacrificial anode, while the products have no effect on the erosion process.

Acknowledgement

5 REFERENCES

[1] M. Emami, H. R. Shahverdi, S. Hayashi, M. J. Torkamany, A combined hot dip aluminizing/laser alloying treatment to produce iron-rich aluminides on alloy steel, Metall. Mater. Trans. A., 44 (**2013**), 3176–3184, doi:10.1007/s11661-013-1666-2

[2] A. R. Rastkar, N. Rezvani, The effects of processing time on the microstructure and composition of plasma pack aluminized and oxidized surface layers on low carbon steel, Metall. Mater. Trans. A., 46 (**2015**), 4132–4142, doi:10.1007/s11661-015-3034-x

[3] A. Soleimani Dorcheh, M. C. Galetz, Slurry aluminizing: A solution for molten nitrate salt corrosion in concentrated solar power plants, Sol. Energ. Mat. Sol. C., 146 (**2016**), 8–15, doi:10.1016/j.solmat.2015.11.024

[4] A. Canakci, T. Varol, F. Erdemir, S. Ozkaya, H. Mindivan, Microstructure and properties of Fe–Al intermetallic coatings on the low carbon steel synthesized by mechanical alloying, Int. J. Adv. Manuf. Tech., 73 (**2014**), 849–858, doi:10.1007/s00170-014-5851-2

[5] H. R. Karimi Zarchi, M. Soltanieh, M. R. Aboutalebi, X. Guo, Kinetic study on NaF-activated pack-aluminizing of pure titanium at 950–1100 °C, T. Nonferr. Metal. Soc., 24 (**2014**) 6, 1959–1968, doi:10.1016/S1003-6326(14)63277-5

[6] A. R. Rastkar, P. Parseh, N. Darvishnia, S. M. M Hadavi, Microstructural evolution and hardness of TiAl₃ and TiAl₂ phases on Ti-45Al-2Nb-2Mn-1B by plasma pack aluminizing, Appl. Surf. Sci., 276 (**2013**), 112–119, doi:10.1016/j.apsusc.2013.03.043

[7] Z. L. Zhan, Z. Liu, J. X. Liu, L. Li, Z. Li, P. B. Liao, Microstructure and high temperature corrosion behaviors of aluminide coatings by low-temperature pack aluminizing process, Appl. Surf. Sci., 256 (**2010**) 12, 3874–3879, doi:10.1016/j.apsusc.2010.01.043

[8] Z. D. Xiang, P. K. Datta, Effects of pack composition on the formation of aluminide coatings on alloy steels at 650 °C, J. Mater. Sci., 40 (**2005**), 1959–1966, doi:10.1007/s10853-005-1217-3

[9] A. Nishimoto, K. Akamatsu, Microstructure and oxidation resistance of Fe₃Al coatings on austenitic stainless steel by spark plasma sintering, Plasma Process. Polym., 6 (**2009**), S941–S943, doi:10.1002/ppap.200932407

[10] M. Emami, S. M. M Hadavi, S. Hayashi, H. R. Shahverdi, High temperature performance of an FeAl laser coated 9Cr1Mo steel, Oxid. Met., 80 (**2013**), 437–451, doi:10.1007/s11085-013-9415-x

[11] D. R. Yan, Y. Yang, Y. C. Dong, X. Chen, L. Wang, Phase transitions of plasma sprayed Fe-Al intermetallic coating during corrosion in molten zinc at 640 °C, Intermetallics, 22 (**2012**), 160–165, doi:10.1016/j.intermet.2011.10.017

[12] Y. Zhou, S. Q. Wang, B. G. Zhang, Q. Y. Zhang, D. Q. Zhou, Relation between tribolayers and wear behavior during dry sliding of Fe-Al hot-dipped coating, Tribol. T., 60 (**2017**) 6, 1078–1087, doi:10.1080/10402004.2016.1259436

[13] X. L. Zhu, Z. J. Yao, X. D. Gu, W. Cong, P. Z. Zhang, Microstructure and corrosion resistance of Fe-Al intermetallic coating on 45 steel synthesized by double glow plasma surface alloying technology, T. Nonferr. Metal. Soc., 19 (**2009**) 1, 143–148, doi:10.1016/s1003-6326(08) 60242-3

[14] A. Canakci, T. Varol, F. Erdemir, S. Ozkaya, H. Mindivan, Microstructure and properties of Fe-Al intermetallic coatings on the low carbon steel synthesized by mechanical alloying, Int. J. Adv. Manuf. Tech., 73 (**2014**), 849–858, doi:10.1007/s00170-014-5851-2

[15] A. H. Seikh, A. Sarkar, J. K. Singh, S. M. A. Khan Mohammed, N. Alharthi, M. Ghosh, Corrosion Characteristics of Copper-Added Austempered Gray Cast Iron (AGCI), Materials, 12 (**2019**) 3, 503, doi:10.3390/ma12030503

[16] N. N. Li, M. Z. Wang, Y. S. Li, G. Chen, P. Li, Corrosion behavior of Fe-Al coatings fabricated by pack aluminizing method, Acta Metall. Sin., 29 (**2016**) 9, 813–819, doi:10.1007/s 40195-016-0455-5

[17] Test Methods for Electrochemical Properties of Sacrificial Anodes, GB/T 17848-1999 (in Chinese)

[18] A. Ashrafi, M. A. Golozar, S. Mallkpour, EIS investigation of passive film formation on mild steel in oxalic acid solution, J. Appl. Electrochem., 38 (**2008**), 225–229, doi:10.1007/s10800-007-9429-7

[19] N. Ahledel, R. Schulz, M. Gariepy, H. Hermawan, H. Alamdari, Electrochemical corrosion behavior of Fe₃Al/TiC and Fe₃Al-Cr/TiC coatings prepared by HVOF in NaCl solution, Metals, 9 (**2019**) 4, 437, doi:10.3390/met 9040437